Differential and total cross sections for antiproton-impact ionization of atomic hydrogen and helium

M. McGovern,[1] D. Assafrão,[2] J. R. Mohallem,[2] Colm T. Whelan,[3] and H. R. J. Walters[1]
[1]*Department of Applied Mathematics and Theoretical Physics, Queen's University, Belfast BT7 1NN, United Kingdom*
[2]*Departamento de Física, Laboratório de Átomos e Moléculas Especiais, ICEx, Universidade Federal de Minas Gerais, P.O. Box 702, 30123-970 Belo Horizonte, MG, Brazil*
[3]*Department of Physics, Old Dominion University, Norfolk, Virginia 23529-0116, USA*
(Received 15 January 2009; published 6 April 2009)

We develop a method for extracting fully differential cross sections for ionization from an impact-parameter treatment of the collision. The approach uses pseudostates. The method is applied to antiproton-impact ionization of H and He. It is not restricted to antiprotons but can be used with other projectiles. The method automatically includes the interaction between the projectile and the target nucleus. This interaction is shown to be very important in low-energy antiproton ionization. Integrated cross sections for elastic scattering, discrete excitation, ionization, and total scattering are also calculated. For ionization, these are compared with experimental data on H and He. At impact energies greater than 30 keV there is agreement with these data. At lower energies the calculated cross sections for He are in disagreement with the trend of the older experimental data of Andersen *et al.* and Hvelplund *et al.* but are in qualitative accord with the recent measurement of Knudsen *et al.* However, there is no overall quantitative agreement with the new measurements. First-order Born calculations are also presented as a benchmark for checking the pseudostate approximation.

DOI: 10.1103/PhysRevA.79.042707 PACS number(s): 34.10.+x, 34.50.Fa

I. INTRODUCTION

The main thrust of this paper is directed towards differential cross sections for single ionization of atomic hydrogen and helium and with particular reference to the most detailed cross section, the triple differential cross section (TDCS). We show how, within a coupled pseudostate (CP) formalism, the TDCS can be extracted from an impact-parameter treatment. By-products of this work are cross sections for total ionization and discrete excitation of the atom. While there is not so much work on differential ionization [1–8], there is a large body of literature on the total ionization cross section [4–6,8–44]. Here we largely confirm what has gone before but, we believe, with some significant insights.

In Sec. II we derive an approximation which is fully differential in the motion of the "heavy" projectile and the ionized electron. Here, using perturbation theory, we establish a connection between the wave treatment of projectile motion and the straight-line impact-parameter method (IPM). This enables us to describe the deflection of the heavy projectile even though the straight-line IPM seemingly does not allow such. Next we show how differential electron ejection can be obtained from the pseudostates. Combining this with the results for projectile deflection we are able to construct an amplitude that is fully differential in both particles.

As a useful benchmark to judge the coupled pseudostate results we also calculate first-order Born cross sections in the wave treatment (Sec. III). By setting all couplings to zero except those that connect to the initial atomic state and by decoupling the initial state from itself, the coupled IPM equations can be run in first Born mode. Comparison with the corresponding first Born wave treatment then enables us to judge how well the pseudostates are performing in representing the ionized electron continuum as well as the validity of the IPM, at least at the first Born level. The first Born calculations also clearly define the asymptotic limit to which the coupled pseudostate results should converge with increasing impact energy.

Our results are presented in Sec. IV where comparison is made with the available experimental data on total ionization. This gives us the opportunity to assess some very recent new measurements on helium [45] which show a completely different trend to the earlier data [46,47] at the lower impact energies. Conclusions are summarized in Sec. V.

Throughout we use atomic units (a.u.) in which $\hbar = m_e = e = 1$.

II. THEORY

We consider a bare charged particle of mass m_P and charge Z_P incident with velocity $\mathbf{v}_0$ upon an N-electron neutral atom of nuclear mass m_T which is at rest in the laboratory. It is convenient to work in the relative coordinate system in which the target remains at rest throughout the collision and the projectile has an effective (reduced) mass of

$$\mu = \frac{m_P(m_T + N)}{(m_P + m_T + N)}.$$

We denote by $\mathbf{R}(\mathbf{r}_i)$ the position vector of the projectile (ith electron) relative to the target nucleus and by $\mathbf{r}$ and $\mathbf{X}$ the collective coordinates $\mathbf{r} \equiv (\mathbf{r}_1, \mathbf{r}_2, \ldots, \mathbf{r}_N)$ and $\mathbf{X} \equiv (\mathbf{x}_1, \mathbf{x}_2, \ldots, \mathbf{x}_N)$, where $\mathbf{x}_i \equiv (\mathbf{r}_i, s_i)$ and s_i is the spin coordinate of the ith electron. Let H_A be the atomic Hamiltonian and $V(\mathbf{r}, \mathbf{R})$ the Coulombic interaction between the projectile and the target:

$$H_A \equiv \sum_{i=1}^{N} \left(-\frac{1}{2}\nabla_i^2 - \frac{Z_T}{r_i} \right) + \sum_{\substack{i,j=1 \\ i<j}}^{N} \frac{1}{|\mathbf{r}_i - \mathbf{r}_j|}, \qquad (1)$$

$$V(\mathbf{r},\mathbf{R}) \equiv \frac{Z_p Z_T}{R} - \sum_{i=1}^{N} \frac{Z_P}{|\mathbf{R}-\mathbf{r}_i|}. \tag{2}$$

We emphasize that V includes the interaction between the projectile and target nucleus as well as the interaction between the projectile and target electrons. Often in treatments of heavy particle collisions the former is ignored, it being argued that it can be transformed away as an overall phase factor.

A. Impact-parameter treatment

In the IPM it is assumed that the projectile moves along a straight-line path with the incident speed v_0 and at perpendicular distance b (the impact parameter) from the stationary target. Let the z direction be the direction of the path and write

$$\mathbf{R} = v_0 t\hat{\mathbf{k}} + \mathbf{b}, \tag{3}$$

where t is the time ($t=0$ being the time of closest approach) and $\hat{\mathbf{k}}$ is a unit vector in the z direction. Let Ψ be the wave function describing the motion of the target electrons. It satisfies the time-dependent Schrödinger equation, i.e.,

$$(H_A + V)\Psi = i\frac{\partial \Psi}{\partial t}. \tag{4}$$

We expand Ψ in atom states $\psi_\alpha(\mathbf{X})$,

$$\Psi = \sum_\alpha a_\alpha(t,\mathbf{b}) e^{-i\varepsilon_\alpha t}\psi_\alpha(\mathbf{X}), \tag{5}$$

where we assume that the states ψ_α are orthonormal and diagonalize the atomic Hamiltonian according to

$$\langle \psi_\alpha | H_A | \psi_\beta \rangle = \varepsilon_\alpha \delta_{\alpha\beta}. \tag{6}$$

The states ψ_α may be discrete eigenstates ($H_A\psi_\alpha = \varepsilon_\alpha \psi_\alpha$) or pseudostates satisfying Eq. (6). Pseudostates are a way of representing the atomic continuum in discrete form. Note that Eq. (5) is a single-center expansion based on the target atom and so makes no explicit allowance for charge exchange to the projectile. This is reasonable when the projectile is a negatively charged antiproton or for a positively charged projectile at an impact energy high enough for charge exchange to be negligible. Substitution of Eq. (5) into Eq. (4) and projection with ψ_α leads to the usual coupled equations,

$$i\frac{da_\alpha}{dt} = \sum_\beta e^{i(\varepsilon_\alpha - \varepsilon_\beta)t}\langle \psi_\alpha | V | \psi_\beta \rangle a_\beta. \tag{7}$$

If the atom is initially in the state ψ_0 then these equations must be solved subject to the boundary conditions,

$$a_\alpha(-\infty,\mathbf{b}) = \delta_{\alpha 0}. \tag{8}$$

If the states ψ_α are quantized along the z direction then it is not difficult to show that

$$V_{\alpha\beta}(\mathbf{R}) \equiv \langle \psi_\alpha | V | \psi_\beta \rangle = \bar{V}_{\alpha\beta}(b,Z) e^{i(m_\beta - m_\alpha)\phi_b}, \tag{9}$$

where $Z=v_0 t$ is the z coordinate of $\mathbf{R}$, ϕ_b is the azimuthal angle of $\mathbf{b}$ (equivalently $\mathbf{R}$) about the z direction, and m_α is the azimuthal (magnetic) quantum number of the state ψ_α. Defining

$$\bar{a}_\alpha \equiv e^{i m_\alpha \phi_b} a_\alpha, \tag{10}$$

Eq. (7) become

$$i\frac{d\bar{a}_\alpha}{dt} = \sum_\beta e^{i(\varepsilon_\alpha - \varepsilon_\beta)t}\bar{V}_{\alpha\beta}(b,Z)\bar{a}_\beta. \tag{11}$$

If these are solved subject to the boundary condition

$$\bar{a}_\alpha = \delta_{\alpha 0} \quad \text{at} \quad t = -\infty, \tag{12}$$

then the resulting solutions will have no dependence on ϕ_b, i.e., $\bar{a}_\alpha \equiv \bar{a}_\alpha(t,b)$. Then, from Eq. (10), the solution of Eq. (7) subject to Eq. (8) will be

$$a_\alpha(t,\mathbf{b}) = e^{i(m_0 - m_\alpha)\phi_b}\bar{a}_\alpha(t,b). \tag{13}$$

Assuming Condon-Shortley phase conventions [48], it can also be shown that

$$\bar{V}_{\alpha',-m_\alpha;\beta',-m_\beta} = (-1)^{m_\beta - m_\alpha}\bar{V}_{\alpha' m_\alpha;\beta' m_\beta}, \tag{14}$$

where we write $\alpha \equiv \alpha' m_\alpha$, α' standing for quantum numbers other than m_α needed to label the state ψ_α. From Eqs. (11) and (14) it follows that

$$\bar{a}_{\alpha',-m_\alpha} = (-1)^{m_a}\bar{a}_{\alpha' m_\alpha} \tag{15}$$

if $m_0=0$ and where we assume that the sum over β in Eq. (11) includes both $\beta', -m_\beta$ and $\beta' m_\beta$. Condition (15) means that, in this case, we need only concern ourselves with nonnegative values of m_α and m_β when solving Eq. (11):

$$i\frac{d\bar{a}_{\alpha' m_\alpha}}{dt} = \sum_{\beta' m_\beta}\left(1 - \frac{\delta_{m_\beta 0}}{2}\right)e^{i(\varepsilon_{\alpha'} - \varepsilon_{\beta'})t} \times [\bar{V}_{\alpha' m_\alpha;\beta' m_\beta} + (-1)^{m_\beta}\bar{V}_{\alpha' m_\alpha;\beta' -m_\beta}]\bar{a}_{\beta' m_\beta},$$

$$m_\beta \geq 0, \quad m_\alpha \geq 0, \quad m_0 = 0. \tag{16}$$

B. Extraction of differential scattering of the projectile

It might seem that the straight-line IPM discussed in Sec. IIA could not describe deflection of the projectile but that would be to misunderstand the IPM. To see the connection we go to the wave treatment. In the wave approach, and in the relative coordinate system in which the target is treated as if it were at rest, the differential cross section for scattering of the projectile is given by

$$\frac{d\sigma_{f0}}{d\Omega_p} = \mu^2 \frac{k_f}{k_0}|f_{f0}|^2, \tag{17}$$

where

$$f_{f0} = -\frac{1}{2\pi}\langle e^{i\mathbf{k}_f\cdot\mathbf{R}}\psi_f(\mathbf{X})|V|\Psi^+\rangle, \tag{18}$$

$$\Psi^+ \xrightarrow{R\sim\infty} e^{i\mathbf{k}_0\cdot\mathbf{R}}\psi_0(\mathbf{X}) + (\text{outgoing scattered waves}). \tag{19}$$

In Eqs. (17)–(19) $d\Omega_p$ is the solid angle into which the projectile is scattered (in the relative coordinate system), $\psi_f(\psi_0)$ is the final (initial) state of the atom,

$$\mu = \frac{m_P(m_T+N)}{(m_P+m_T+N)}$$

is the reduced mass of the projectile and target, $\mathbf{k}_0(\mathbf{k}_f)$ is the initial (final) relative momentum of the projectile, and Ψ^+ is the full scattering wave function. Since we assume that in the laboratory the projectile is incident with velocity $\mathbf{v}_0$ upon a stationary target, $\mathbf{k}_0=\mu\mathbf{v}_0$. Analogously $\mathbf{k}_f=\mu\mathbf{v}_f$, where $\mathbf{v}_f$ is the velocity of the projectile relative to the target after the collision.

First let us look at a perturbative solution of the IPM Eqs. (7) and (8). The first-order (first Born) approximation gives

$$a_\alpha^{B1}(t,\mathbf{b}) = \delta_{\alpha 0} - i\int_{-\infty}^{t} e^{i(\varepsilon_\alpha-\varepsilon_0)t'}\langle\psi_\alpha|V(\mathbf{r},v_0t'\hat{\mathbf{k}}+\mathbf{b})|\psi_0\rangle dt'. \tag{20}$$

The second-order approximation is $a_\alpha^{B1}+a_\alpha^{B2}$ where the second Born term is given by

$$a_\alpha^{B2}(t,\mathbf{b}) = -\sum_\beta \int_{-\infty}^{t} dt' e^{i(\varepsilon_\alpha-\varepsilon_\beta)t'}\langle\psi_\alpha|V(\mathbf{r},v_0t'\hat{\mathbf{k}}+\mathbf{b}) \times|\psi_\beta\rangle\int_{-\infty}^{t'} dt'' e^{i(\varepsilon_\beta-\varepsilon_0)t''}\langle\psi_\beta|V(\mathbf{r},v_0t''\hat{\mathbf{k}}+\mathbf{b})|\psi_0\rangle. \tag{21}$$

Now consider the Born series approximation to Eq. (18). In first order we have

$$f_{f0}^{B1} = -\frac{1}{2\pi}\langle e^{i\mathbf{k}_f\cdot\mathbf{R}}\psi_f|V|e^{i\mathbf{k}_0\cdot\mathbf{R}}\psi_0\rangle. \tag{22}$$

Choosing a z axis in the direction of $\mathbf{k}_0+\mathbf{k}_f$ [49] and writing

$$\mathbf{R} = Z\hat{\mathbf{k}} + \mathbf{b}, \tag{23}$$

where

$$\hat{\mathbf{k}} \equiv \frac{\mathbf{k}_0+\mathbf{k}_f}{|\mathbf{k}_0+\mathbf{k}_f|}, \quad \hat{\mathbf{k}}\cdot\mathbf{b} = 0, \tag{24}$$

the plane wave terms in Eq. (22) may be rendered as

$$e^{i\mathbf{q}\cdot\mathbf{b}}e^{i\mathbf{q}\cdot\hat{\mathbf{k}}Z}, \tag{25}$$

where $\mathbf{q}\equiv\mathbf{k}_0-\mathbf{k}_f$ is the momentum transfer in the collision. From Eq. (24)

$$\mathbf{q}\cdot\hat{\mathbf{k}} = \frac{k_0^2-k_f^2}{|\mathbf{k}_0+\mathbf{k}_f|} = \frac{2\mu(\varepsilon_f-\varepsilon_0)}{|\mathbf{k}_0+\mathbf{k}_f|} \tag{26}$$

by conservation of energy. So far, no approximation has been made. Typically $(\varepsilon_f-\varepsilon_0)$ will be a few a.u., while, if the projectile is an antiproton or ion, μ will be 1000 s of a.u.. Consequently, except at low energies (less than about 1 keV for antiproton impact) we may assume that $k_f\approx k_0$. Furthermore, in the same situation the deflection of the projectile will be typically milliradians, and so it is reasonable to approximate

$$|\mathbf{k}_0+\mathbf{k}_f| \to 2k_0 = 2\mu v_0. \tag{27}$$

Introducing the variable $t=\frac{Z}{v_0}$, Eq. (22) under approximation (27) becomes

$$f_{f0}^{B1} = -\frac{v_0}{2\pi}\int\left\{\int_{-\infty}^{+\infty} e^{i(\varepsilon_f-\varepsilon_0)t}\langle\psi_f|V(\mathbf{r},v_0t\hat{\mathbf{k}}+\mathbf{b})|\psi_0\rangle dt\right\} \times e^{i\mathbf{q}\cdot\mathbf{b}}d^2\mathbf{b} = -\frac{v_0 i}{2\pi}\int e^{i\mathbf{q}\cdot\mathbf{b}}[a_f^{B1}(\infty,\mathbf{b})-\delta_{f0}]d^2\mathbf{b} \tag{28}$$

using Eq. (20).

Let us now look at the second Born term in the wave treatment:

$$f_{f0}^{B2} = -\frac{\mu}{8\pi^4}\lim_{\varepsilon\to 0+}\sum_\beta\int\frac{d\mathbf{k}}{k_\beta^2-k^2+i\varepsilon}\langle e^{i\mathbf{k}_f\cdot\mathbf{R}}\psi_f|V|e^{i\mathbf{k}\cdot\mathbf{R}}\psi_\beta\rangle \times\langle e^{i\mathbf{k}\cdot\mathbf{R}}\psi_\beta|V|e^{i\mathbf{k}_0\cdot\mathbf{R}}\psi_0\rangle, \tag{29a}$$

$$k_\beta^2 \equiv k_0^2 + 2\mu(\varepsilon_0-\varepsilon_\beta). \tag{29b}$$

Consider the propagator

$$k_\beta^2-k^2+i\varepsilon = (k_\beta+k)(k_\beta-k)+i\varepsilon. \tag{30}$$

Typically, k_0, k_f, and k_β in this work will be of the order of 1000 s of a.u. but will differ by a few a.u. $[k_\beta=k_0+[(\varepsilon_0-\varepsilon_\beta)/v_0]+O(\frac{1}{\mu})]$, while the matrix elements will be negligible beyond a few a.u. about $\mathbf{k}_0$ and $\mathbf{k}_f$. Under these circumstances we may approximate $(k_\beta+k)$ by $2k_\beta+O(\frac{1}{\mu})$. Also, under the same conditions, with the z direction along $\mathbf{k}_0+\mathbf{k}_f$, we may approximate $(k_\beta-k)$ by $(k_\beta-k_z)+O(\frac{1}{\mu})$. Overall, therefore, an appropriate approximation to Eq. (29) would be

$$-\frac{\mu}{8\pi^4}\lim_{\varepsilon\to 0+}\sum_\beta\int\frac{dk_z d^2\mathbf{k}}{2k_\beta(k_\beta-k_z)+i\varepsilon}\langle e^{i\mathbf{k}_f\cdot\mathbf{R}}\psi_f|V|e^{i\mathbf{k}\cdot\mathbf{R}}\psi_\beta\rangle \times\langle e^{i\mathbf{k}\cdot\mathbf{R}}\psi_\beta|V|e^{i\mathbf{k}_0\cdot\mathbf{R}}\psi_0\rangle, \tag{31}$$

where $d^2\mathbf{k}\equiv dk_x dk_y$. Geometrically, approximation (31) in $\mathbf{k}$ space amounts to replacing the (very large) sphere $k=k_\beta$ corresponding to the propagator by a plane $k_z=k_\beta$ in the region where the matrix elements have significant size, i.e., perpendicular to $\mathbf{k}_0+\mathbf{k}_f$.

Now consider the exponentials involving $\mathbf{k}$ in Eq. (31) and write

$$e^{i\mathbf{k}\cdot(\mathbf{R}-\mathbf{R}')} = e^{ik_z\cdot(Z-Z')}e^{i\mathbf{k}_b\cdot(\mathbf{b}-\mathbf{b}')}, \tag{32}$$

where $\mathbf{k}=k_z\hat{\mathbf{k}}+\mathbf{k}_b$ with $\mathbf{k}_b\cdot\hat{\mathbf{k}}=0$. Then, using

$$\lim_{\varepsilon\to 0+}\int_{-\infty}^{+\infty}\frac{dk_z}{2k_\beta(k_\beta-k_z)+i\varepsilon}e^{ik_z(Z-Z')}=\begin{cases}-\dfrac{\pi i}{k_\beta}e^{ik_\beta(Z-Z')} & \text{if } Z>Z'\\ 0 & \text{if } Z<Z',\end{cases}\tag{33}$$

and

$$\int d^2\mathbf{k}_b e^{i\mathbf{k}_b\cdot(\mathbf{b}-\mathbf{b}')}=4\pi^2\delta^{(2)}(\mathbf{b}-\mathbf{b}'),\tag{34}$$

Eq. (31) may be written as

$$+\frac{\mu i}{2\pi}\sum_\beta\frac{1}{k_\beta}\int d^2\mathbf{b}e^{i(\mathbf{k}_{0\mathbf{b}}-\mathbf{k}_{fb})\cdot\mathbf{b}}\left\{\int_{-\infty}^{+\infty}dZe^{i(k_\beta-k_{fz})Z}\langle\psi_f|V|\psi_\beta\rangle\right.$$
$$\left.\times\int_{-\infty}^{Z}dZ'e^{i(k_{0z}-k_\beta)Z'}\langle\psi_\beta|V|\psi_0\rangle\right\}.\tag{35}$$

Now

$$k_{0z}=k_0+O\left(\frac{1}{\mu}\right),\quad k_{fz}=k_f+O\left(\frac{1}{\mu}\right),$$
$$k_f=k_0+\frac{(\varepsilon_0-\varepsilon_f)}{v_0}+O\left(\frac{1}{\mu}\right),$$
$$k_\beta=k_0+\frac{(\varepsilon_0-\varepsilon_\beta)}{v_0}+O\left(\frac{1}{\mu}\right).\tag{36}$$

Thus, neglecting terms of $O(\frac{1}{\mu})$, replacing

$$\frac{1}{k_\beta}\to\frac{1}{k_0}=\frac{1}{\mu v_0},\tag{37}$$

and setting $Z=v_0t$, we finally get

$$f_{f0}^{B2}=\frac{v_0 i}{2\pi}\sum_\beta\int d^2\mathbf{b}e^{i\mathbf{q}\cdot\mathbf{b}}\left\{\int_{-\infty}^{+\infty}dte^{i(\varepsilon_f-\varepsilon_\beta)t}\langle\psi_f|V(\mathbf{r},v_0t\hat{\mathbf{k}}+\mathbf{b})\right.$$
$$\left.\times|\psi_\beta\rangle\int_{-\infty}^{t}dt'e^{i(\varepsilon_\beta-\varepsilon_0)t'}\langle\psi_\beta|V(\mathbf{r},v_0t'\hat{\mathbf{k}}+\mathbf{b})|\psi_0\rangle\right\}.\tag{38}$$

Comparison of Eq. (38) with Eq. (21) gives

$$f_{f0}^{B2}=-\frac{v_0 i}{2\pi}\int e^{i\mathbf{q}\cdot\mathbf{b}}a_f^{B2}(\infty,\mathbf{b})d^2\mathbf{b},\tag{39}$$

i.e., exactly the same relationship (ignoring the δ_{f0} which is peculiar to the first-order term) as for the first Born term [Eq. (28)].

Similar approximations in higher-order Born terms lead to the same relationship as Eq. (39). We therefore conclude that, within the given level of approximation, the scattering amplitude in the wave treatment is related to that in the impact-parameter method by, see Eqs. (28) and (39),

$$f_{f0}=-\frac{v_0 i}{2\pi}\int e^{i\mathbf{q}\cdot\mathbf{b}}[a_f(\infty,\mathbf{b})-\delta_{f0}]d^2\mathbf{b}.\tag{40}$$

Using Eq. (13), Eq. (40) may be written as

$$f_{f0}=-\frac{v_0 i}{2\pi}e^{i(m_0-m_f)\phi_q}\int_0^{2\pi}d\Phi\int_0^\infty bdb$$
$$\times e^{iq_tb\cos\Phi}e^{i(m_0-m_f)\Phi}[\bar{a}_f(\infty,b)-\delta_{f0}],\tag{41}$$

where ϕ_q is the azimuthal angle of the vector $\mathbf{q}$ and q_t is the magnitude of its transverse component, i.e., component in the direction perpendicular to z (equivalently $\mathbf{v}_0$ [49]). Employing the Bessel function result [50],

$$\int_0^{2\pi}e^{iq_tb\cos\Phi}e^{i(m_0-m_f)\Phi}d\Phi=2\pi i^{m_f-m_0}J_{(m_f-m_0)}(q_tb),\tag{42}$$

the integral over Φ in Eq. (41) may be performed to leave the single integral formula,

$$f_{f0}=-v_0i^{m_f-m_0+1}e^{i(m_0-m_f)\phi_q}\int_0^\infty J_{(m_f-m_0)}(q_tb)[\bar{a}_f(\infty,b)$$
$$-\delta_{f0}]bdb.\tag{43}$$

While result (43) is known (see [51] and references therein), we believe that the preceding derivation presents some different insights.

C. Extraction of differential electron ejection

We are interested in the case where the final state of the atom, $\psi_f(\mathbf{X})$, is singly ionized. We denote it by $\psi^-_{\boldsymbol{\kappa},i}(\mathbf{X})$, where $\boldsymbol{\kappa}$ is the asymptotic momentum of the ejected electron and the i labels the final state of the ion. $\psi^-_{\boldsymbol{\kappa},i}$ is a scattering state corresponding to an electron incident with momentum $\boldsymbol{\kappa}$ upon the ion in the state i with ingoing scattered wave boundary conditions. We assume that it is normalized according to

$$\langle\psi^-_{\boldsymbol{\kappa},i}|\psi^-_{\boldsymbol{\kappa}',i}\rangle=\delta(\boldsymbol{\kappa}-\boldsymbol{\kappa}').\tag{44}$$

The amplitude [Eq. (18)] corresponding to ionization is therefore

$$f_{\text{ion}}=-\frac{1}{2\pi}\langle e^{i\mathbf{k}_f\cdot\mathbf{R}}\psi^-_{\boldsymbol{\kappa},i}(\mathbf{X})|V|\Psi^+\rangle.\tag{45}$$

Let us assume that our set of states ψ_α, consisting of bound eigenstates and pseudostates, approximates a complete set for matrix element purposes [52]. Then we may write

$$\langle e^{i\mathbf{k}_f\cdot\mathbf{R}}\psi^-_{\boldsymbol{\kappa},i}|V|\Psi^+\rangle=\sum_\alpha\langle\psi^-_{\boldsymbol{\kappa},i}|\psi_\alpha\rangle\langle e^{i\mathbf{k}_f\cdot\mathbf{R}}\psi_\alpha|V|\Psi^+\rangle.\tag{46}$$

We note that the amplitudes $\langle e^{i\mathbf{k}_f\cdot\mathbf{R}}\psi_\alpha|V|\Psi^+\rangle$ in Eq. (46) are in general off-energy shell. Conservation of energy in the ionization process requires that $k_0^2=k_f^2+\mu(\kappa^2+2I_i)$, where I_i is the ionization potential of the initial state ψ_0 leading to the ion state i. Unless deliberately engineered, it is extremely unlikely that for a particular state ψ_α we shall have conservation of energy, i.e., $k_0^2+2\mu\varepsilon_0=k_f^2+2\mu\varepsilon_\alpha$. However let us be deliberate. Let us construct our states ψ_α so that one state from each symmetry (S-, P-, D-, etc.) has exactly the right energy for conservation, i.e., $\varepsilon_\alpha=\frac{\kappa^2}{2}+I_i+\varepsilon_0$. Let us now as-

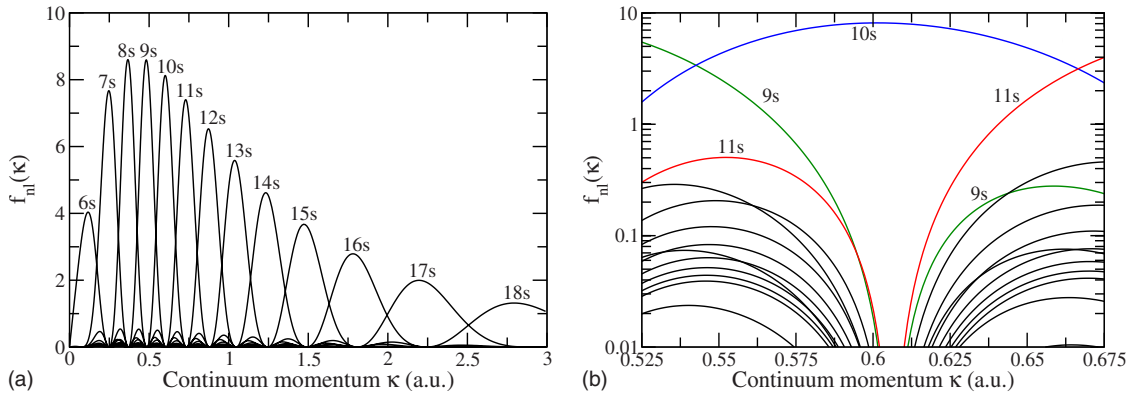

FIG. 1. (Color online) Distribution functions $f_{nl}(\kappa)$ of Eq. (58) for the $6s$ to $18s$ states used in the 165 state calculations of this paper for atomic hydrogen.

sume that only these states make a significant contribution to the sum in Eq. (46) (we shall deal with this point below, see discussion of Fig. 1). We may then write

$$\langle e^{i\mathbf{k}_f\cdot\mathbf{R}}\psi^-_{\boldsymbol{\kappa},i}|V|\Psi^+\rangle \simeq \sum_{\substack{\alpha \\ \varepsilon_\alpha=\frac{\kappa^2}{2}+I_i+\varepsilon_0}} \langle\psi^-_{\boldsymbol{\kappa},i}|\psi_\alpha\rangle\langle e^{i\mathbf{k}_f\cdot\mathbf{R}}\psi_\alpha|V|\Psi^+\rangle. \tag{47}$$

Since the amplitudes $\langle e^{i\mathbf{k}_f\cdot\mathbf{R}}\psi_\alpha|V|\Psi^+\rangle$ are now on-energy shell, we may use Eqs. (18) and (43) to relate them to the impact-parameter coefficients $\bar{a}_\alpha(\infty,b)$.

To proceed further we must address the particular targets of interest to us.

1. Atomic hydrogen target

Here $\psi^-_{\boldsymbol{\kappa},i}\equiv\psi^-_{\boldsymbol{\kappa}}$ [53] is the pure Coulomb wave [54],

$$\psi^-_{\boldsymbol{\kappa}} = \sqrt{\frac{2}{\pi}}\sum_{l,m} i^l e^{-i\eta^c_l} U_l(\kappa,r) Y^*_{lm}(\hat{\boldsymbol{\kappa}}) Y_{lm}(\hat{\mathbf{r}}), \tag{48}$$

where

$$U_l(\kappa,r) \xrightarrow{r\sim\infty} \frac{\sin\left(\kappa r - \frac{1}{2}l\pi - \alpha\ln 2\kappa r + \eta^c_l\right)}{\kappa r}, \tag{49}$$

$$\alpha \equiv -\frac{1}{\kappa}, \tag{50}$$

and η^c_l is the Coulomb phase shift given by

$$\eta^c_l = \arg\Gamma(l+1+i\alpha). \tag{51}$$

Using hydrogenic notation ψ_{nlm} [55] for the states ψ_α, we separate them into radial and angular components according to

$$\psi_{nlm}(\mathbf{r}) = R_{nl}(r)Y_{lm}(\hat{\mathbf{r}}). \tag{52}$$

It then follows that

$$\langle\psi^-_{\boldsymbol{\kappa}}|\psi_{nlm}\rangle = \sqrt{\frac{2}{\pi}}(-i)^l e^{i\eta^c_l} b_{nl}(\kappa) Y_{lm}(\hat{\boldsymbol{\kappa}}), \tag{53}$$

where $b_{nl}(\kappa)$ is the real quantity,

$$b_{nl}(\kappa) \equiv \int_0^\infty U_l(\kappa,r)R_{nl}(r)r^2dr. \tag{54}$$

Then, using Eqs. (43), (45), (47), and (53), we get as our approximation to the ionization amplitude

$$f_{\text{ion}} = -\sqrt{\frac{2}{\pi}}v_0\sum_l (-i)^l e^{i\eta^c_l} b_{\bar{n}l}(\kappa) \times \sum_{m=-l}^{+l} i^{m-m_0+1} C_{\bar{n}lm}(q_t) e^{i(m_0-m)\phi_q} Y_{lm}(\hat{\boldsymbol{\kappa}}), \tag{55}$$

where

$$C_{nlm}(q_t) \equiv \int_0^\infty J_{(m-m_0)}(q_t b)\bar{a}_{nlm}(\infty,b)bdb \tag{56}$$

and $\bar{n}$ labels those pseudostates which have been constructed to have energy $\frac{\kappa^2}{2}$.

At this point it is useful to address the approximation (47) of restricting the sum in Eq. (46) only to those states ψ_α with the same energy as $\psi^-_{\kappa,i}$. As remarked elsewhere [52,56], pseudostates may be considered as "clumps" or "distributions" of eigenstates. From Eq. (53) the fraction of the state ψ_{nlm} lying in the continuum may be calculated as

$$\int |\langle\psi^-_{\boldsymbol{\kappa}}|\psi_{nlm}\rangle|^2 d\boldsymbol{\kappa} = \int_0^\infty \frac{2}{\pi}|b_{nl}(\kappa)|^2\kappa^2 d\kappa. \tag{57}$$

The function

$$f_{nl}(\kappa) = \frac{2\kappa^2}{\pi}|b_{nl}(\kappa)|^2 \tag{58}$$

therefore gives the distribution of the state ψ_{nlm} over the continuum momentum κ. Figure 1(a) shows distributions for the s pseudostates used in the 165 state calculations of Sec. IVA for atomic hydrogen. We note first the idea that the pseudostates divide the continuum up into clumps, but we

also see a more interesting feature. At a momentum κ_{ns} corresponding to a state energy, i.e., $\frac{\kappa_{ns}^2}{2}=\varepsilon_{ns}$, the distribution functions for the remaining states are negligible, i.e., $f_{n's}(\kappa_{ns})\approx 0$ for $n'\neq n$. We have found this also to be true for nonzero angular momenta and for a much smaller set of H states generated with a different form of basis [57], as well as for the He target discussed in this work. The point is illustrated more forcibly in Fig. 1(b) where we show the distributions on a logarithmic scale in the vicinity of the 10 s state which was constructed to have an energy of 5 eV ($\kappa_{10s}=0.6062$ a.u.). The plunging of the distribution functions for the other states at this point is most pronounced. We are tempted to suggest that, maybe, $f_{nl}(\kappa_{n'l})$ is identically zero if $n'\neq n$ although, at present, we can see no way to prove such a result. It is certainly trivially true in the asymptotic limit where the number of states tends to infinity and the states become exact continuum eigenstates. For present purposes, however, the important point is that the approximation step of Eq. (47) is extremely good (if not exact were our conjecture correct). The real approximation in extracting the differential ejection from Ψ^+ is step (46) where it is assumed that the pseudostates form a complete set for matrix element purposes.

2. Helium target

For the states ψ_α of He we adopt a frozen-core approximation in which one of the electrons is frozen into the $1s$ orbital, ϕ_{1s}^+, of He^+. Since the total electronic spin of the He is conserved in the collisions studied here, we need only to deal with the spatial part of ψ_α:

$$\psi_\alpha \equiv \psi_{nlm}(\mathbf{r}_1,\mathbf{r}_2)=\frac{1}{\sqrt{2}}[\phi_{nlm}(\mathbf{r}_1)\phi_{1s}^+(\mathbf{r}_2) + (-1)^S\phi_{nlm}(\mathbf{r}_2)\phi_{1s}^+(\mathbf{r}_1)], \tag{59}$$

where S is the total electronic spin (=0 or 1) and where, since only one electron can be excited, we may use the hydrogenic notation nlm to label the state. The states ψ_{nlm} are orthonormal and satisfy Eq. (6). Consistent with Eq. (59), we approximate the continuum eigenfunction $\psi_{\boldsymbol{\kappa},i}^-\equiv\psi_{\boldsymbol{\kappa}}^-$ as

$$\psi_{\boldsymbol{\kappa}}^-=\frac{1}{\sqrt{2}}[F(\mathbf{r}_1)\phi_{1s}^+(\mathbf{r}_2)+(-1)^SF(\mathbf{r}_2)\phi_{1s}^+(\mathbf{r}_1)]. \tag{60}$$

Substituting Eq. (60) into the Schrödinger equation for He and projecting with ϕ_{1s}^+, we obtain a coupled integrodifferential equation for $F(\mathbf{r})$ which is solved subject to the boundary condition

$$F(\mathbf{r})\xrightarrow{r\sim\infty}\frac{1}{(2\pi)^{3/2}}\left[1-\frac{\alpha^2}{i(\kappa r+\boldsymbol{\kappa}\cdot\mathbf{r})}\right]e^{i\boldsymbol{\kappa}\cdot\mathbf{r}-i\alpha\, ln(\kappa r+\boldsymbol{\kappa}\cdot\mathbf{r})} + (\text{ingoing scattered waves}). \tag{61}$$

Approximation (60) corresponds to $e^-(\boldsymbol{\kappa})+He^+(1s)$ scattering in the static-exchange approximation. Expanding $F(\mathbf{r})$ in partial waves as in Eqs. (48) and (49), where now $\eta_l^c\rightarrow\eta_l^{se}$, where η_l^{se} is the phase shift in the static-exchange approximation, and writing ϕ_{nlm} as in Eq. (52), we obtain for $\langle\psi_{\boldsymbol{\kappa}}^-|\psi_{nlm}\rangle$ the same formula as in Eq. (53) but with $\eta_l^c\rightarrow\eta_l^{se}$ and $b_{nl}(\kappa)$ now defined as

$$b_{nl}(\kappa)=\langle\phi_{1s}^+|\phi_{1s}^+\rangle\int_0^\infty U_l(\kappa,r)R_{nl}(r)r^2dr + (-1)^S\delta_{l0}\langle\phi_{1s}^+|\phi_{nlm}\rangle\int_0^\infty U_l(\kappa,r)R^+(r)r^2dr, \tag{62}$$

where $\phi_{1s}^+(\mathbf{r})=\frac{R^+(r)}{\sqrt{4\pi}}$. The formula for the ionization amplitude is then the same as Eq. (55) but with $\eta_l^c\rightarrow\eta_l^{se}$.

Note that our approximation only allows for ionization into the $He^+(1s)$ state, i.e., there is no contribution from ionization with excitation of the ion.

D. Cross sections

The most detailed cross section for ionization is the TDCS,

$$\frac{d^3\sigma}{dEd\Omega_ed\Omega_p}. \tag{63}$$

This is the cross section for the electron being ejected with energy in the range E to $E+dE$ and into the solid angle $d\Omega_e$, while the antiproton is scattered into the solid angle $d\Omega_p$. It is important to define the frame of reference to which Eq. (63) applies. In the relative coordinate system the TDCS [Eq. (63)] is given by

$$\frac{d^3\sigma}{dEd\Omega_ed\Omega_p}=\frac{v_f\kappa}{v_0}\mu^2|f_{\text{ion}}|^2. \tag{64}$$

However, as observed in the laboratory, where we assume that the target is initially at rest, it is

$$\frac{d^3\sigma^L}{dEd\Omega_ed\Omega_p}=\frac{v_f\kappa}{v_0}m_P^2|f_{\text{ion}}|^2. \tag{65}$$

Whereas, under the conditions studied here, dE and $d\Omega_e$ are essentially the same in the relative and laboratory frames, $d\Omega_p$ is different by a factor of $\frac{m_P^2}{\mu^2}$.

Also of interest to us are the double differential cross sections (DDCS) $\frac{d^2\sigma}{dEd\Omega_e}$ and $\frac{d^2\sigma}{dEdq}$, where $q=|\mathbf{k}_0-\mathbf{k}_f|$ is the magnitude of the momentum transfer in the collision. The former is defined by

$$\frac{d^2\sigma}{dEd\Omega_e}=\int\frac{d^3\sigma}{dEd\Omega_ed\Omega_p}d\Omega_p \tag{66}$$

and is negligibly different between the relative and laboratory frames. Using Eq. (55), it is not difficult to perform the integration over $d\Omega_p$ and to show that

$$\frac{d^2\sigma}{dEd\Omega_e}=4\kappa\int_{q_{\min}}^{q_{\max}}qdq\sum_{l,l'}i^{l'-l}e^{i(\eta_l-\eta_{l'})} \times b_{\bar{n}l}(\kappa)b_{\bar{n}l'}(\kappa)\sum_{m=-\min(l,l')}^{+\min(l,l')}C_{\bar{n}lm}(q_t) \times C_{\bar{n}l'm}^*(q_t)P_{lm}(\theta_e)P_{l'm}(\theta_e), \tag{67}$$

where θ_e is the polar ejection angle of the electron, P_{lm} is the associated Legendre function [48], and $\eta_l = \eta_l^c(\eta_l^{se})$ for H (He). The integral in Eq. (67) is over the magnitude of the momentum transfer q from $q_{\min} = |k_0 - k_f|$ to $q_{\max} = |k_0 + k_f|$. Note that, with the z direction as defined in Eq. (24), the magnitude of the transverse momentum transfer q_t can be expressed in terms of q as [58]

$$q_t^2 = q^2 - \frac{4\mu^2(\varepsilon_0 - \varepsilon_f)^2}{2k_0^2 + 2k_f^2 - q^2}, \tag{68a}$$

$$= q^2 - \frac{(\varepsilon_0 - \varepsilon_f)^2}{v_0^2} + O\left(\frac{1}{\mu}\right). \tag{68b}$$

The second DDCS, $\frac{d^2\sigma}{dEdq}$, may be calculated as

$$\frac{d^2\sigma}{dEdq} = \frac{q}{k_0 k_f}\int_0^{2\pi} \frac{d^2\sigma}{dEd\Omega_p} d\phi_p, \tag{69}$$

where

$$\frac{d^2\sigma}{dEd\Omega_p} = \int \frac{d^3\sigma}{dEd\Omega_e d\Omega_p} d\Omega_e \tag{70}$$

and ϕ_p is the azimuthal angle of the outgoing projectile. Using Eq. (55), it is easy to show that

$$\frac{d^2\sigma}{dEdq} = 4q\kappa \sum_l |b_{\bar{n}l}(\kappa)|^2 \sum_{m=-l}^{+l} |C_{\bar{n}lm}(q_t)|^2. \tag{71}$$

The result [Eq. (71)] is negligibly different between the relative and laboratory frames. Indeed, the momentum transfer $\mathbf{q}$ is an invariant, having the same value in the relative and laboratory frames, i.e., $\mathbf{q} = \mu(\mathbf{v}_0 - \mathbf{v}_f) = m_P(\mathbf{v}_0^L - \mathbf{v}_f^L)$, where L labels the velocity in the laboratory frame.

As usual in the impact-parameter method, the total cross section for scattering to any final state ψ_{nlm} is given by

$$\sigma_{nlm} = 2\pi \int_0^\infty |\bar{a}_{nlm}(\infty, b) - \delta_{nlm,n_0 l_0 m_0}|^2 b db, \tag{72}$$

where $n_0 l_0 m_0$ in the initial state. To extract the total ionization cross section we use the result

$$\sigma_{\text{ion}} = \sum_{\text{all nlm}} g_{nl}\sigma_{nlm}, \tag{73}$$

where g_{nl} is the fraction of the state ψ_{nlm} lying in the continuum and is given by Eq. (57).

Finally, the total cross section, σ_{tot}, is calculated from

$$\sigma_{\text{tot}} = \sum_{\text{all } nlm} \sigma_{nlm}. \tag{74}$$

III. CALCULATIONAL DETAILS AND CONVENTIONS

Unless otherwise stated, the calculations reported in this paper, for both H and He, have been made with a basis of 165 states [$l=0-9$, $n=l+1$ to 21, see Eqs. (52) and (59)]. The initial state has been taken to be the ground state [H($1s$) and He(1^1S)] so that, with m values taken into account, we must solve 825 complex coupled equations. (equivalently 1650 real coupled equations). The states have been constructed so that the energy of the $n=10$ states is exactly 5 eV. All of our differential studies are therefore for an electron ejected with 5 eV.

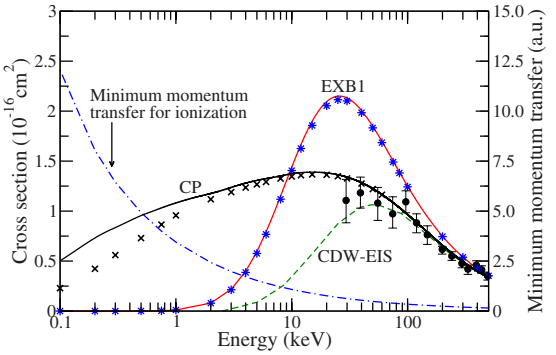

FIG. 2. (Color online) Total ionization cross section for antiproton impact on atomic hydrogen: CP, coupled pseudostate IPM calculation with 165 states; ×, coupled pseudostate IPM calculation with 75 states; EXB1, exact first Born cross section; *, IPMB1 cross section using 165 states; CDW-EIS, continuum distorted wave eikonal initial-state approximation from [15]; solid circles, experimental data from [64]; -.-.-, minimum momentum transfer for ionization.

The H states have been calculated by diagonalization of the atomic Hamiltonian in a basis of Laguerre functions [59], i.e.,

$$\chi_{klm}(\mathbf{r}) = (\lambda_l r)^l L_{k-1}^{2l+2}(\lambda_l r) e^{-\lambda_l r/2} Y_{lm}(\hat{\mathbf{r}}),$$

$$k = 1 \text{ to } (21 - l), \quad l = 0 - 9, \tag{75}$$

with $\lambda_l = 1.8793, 1.9317, 2.0221, 2.1427, 2.2938, 2.4808, 2.7162, 3.0239, 3.4560, 4.1643$ for $l=0-9$, respectively (so that the $n=10$ states have an energy of 5 eV exactly) [60]. The He singlet states have been similarly constructed from a basis [see Eq. (59)],

$$\frac{1}{\sqrt{2}}[\chi_{klm}(\mathbf{r}_1)\phi_{1s}^+(\mathbf{r}_2) + \chi_{klm}(\mathbf{r}_2)\phi_{1s}^+(\mathbf{r})],$$

$$k = 1 \text{ to } (21 - l), \quad l = 0 - 9, \tag{76}$$

where now $\lambda_l = 1.9122, 1.9243, 2.0217, 2.1428$ for $l=0-3$ and is identical to H for $l=4-9$ [61]. With the above choices we find that, for H, the $n=1$ and 2 states are excellent approximations to the corresponding H eigenstates, while the $n=3$ states are very close to the $n=3$ eigenstates and may be treated as such. For He we get a ground-state energy of −2.8725 a.u. which is to be compared with the recommended value of −2.9036 a.u. [62]. This is as good as can be obtained in the frozen-core approximation and gives an ionization potential which is 96.6% of the recommended value. For the $n=2$ and 3 states we get energies (recommended values [62]), in a.u., of −2.1434 (−2.1460) for 2^1S, −2.0606 (−2.0613) for 3^1S, −2.1224 (−2.1238) for 2^1P, −2.0547 (−2.0551) for 3^1P, and −2.0555 (−2.0556) for 3^1D. As in the

case of H, we therefore feel satisfied in treating excitation of the $n=2$ and 3 states as a reasonable approximation to excitation of the exact eigenstates. In our impact-parameter calculations for He we have used our computed energies rather than the recommended values.

We have also performed calculations for H and He using a reduced set of 75 states ($l=0-5$, $n=l+1$ to 15, with the $n=7$ states chosen to have an energy of 5 eV) in order to give some feeling for convergence.

To illuminate our coupled state results [Eq. (16)] we have also calculated first Born cross sections. In the case of atomic hydrogen we are fortunate in having an exact analytic expression for the first Born TDCS in the full wave treatment. It is (using results from [63])

$$\frac{d^3\sigma^L}{dEd\Omega_e d\Omega_p} = \frac{256 v_f m_P^2}{v_0 q^2 \pi (1-e^{-2\pi/\kappa})} \frac{\exp\left[-\frac{2}{\kappa}\tan^{-1}\left(\frac{2\kappa}{1+q^2-\kappa^2}\right)\right]\left[q^2+2(\boldsymbol{\kappa}\cdot\mathbf{q})+\frac{(\kappa^2+1)}{\kappa^2 q^2}(\boldsymbol{\kappa}\cdot\mathbf{q})^2\right]}{[(1+q^2-\kappa^2)^2+4\kappa^2][1+q^2+\kappa^2+2\boldsymbol{\kappa}\cdot\mathbf{q}]^4}. \tag{77}$$

We shall refer to calculations using Eq. (77) as EXB1. Note that Eq. (77) does not involve the use of partial waves. We can also calculate the first Born TDCS in the impact-parameter treatment with pseudostates by using Eq. (55) with $\bar{a}_{nlm}$ in Eq. (56) replaced by $\bar{a}_{nlm}^{B1}$ as calculated according to Eqs. (13) and (20). We shall refer to results evaluated in this way as IPMB1. A comparison of EXB1 and IPMB1 triple differential cross sections will reflect upon the ability of the pseudostate approximation [Eq. (55)] to represent differential ionization, upon whether enough angular momenta l have been included in the pseudostate set for the case considered and upon the suitability of the impact-parameter approximation (28) at the first Born level for the given incident energy. If we integrate Eq. (77) to calculate the first Born total ionization cross section then comparison can also be made with Eq. (73) at the first Born level, again reflecting upon the approximations made in Eq. (73).

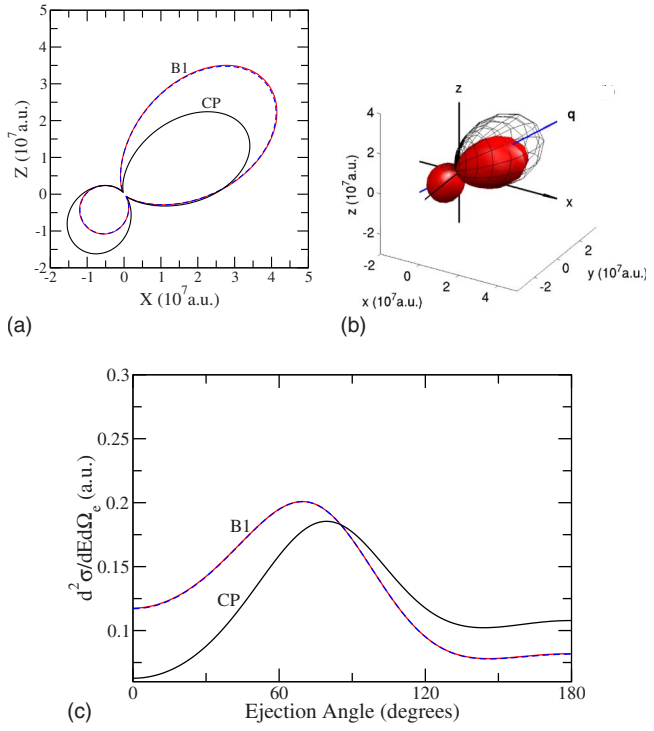

FIG. 3. (Color online) Laboratory frame cross sections (in a.u.) for antiproton ionization of atomic hydrogen at 500 keV and for an ejected electron energy of 5 eV: (a) polar plot of TDCS in scattering plane ($q=0.25$ a.u.); (b) three-dimensional (3D) plot of TDCS ($q=0.25$ a.u.); (c) $d^2\sigma/dEd\Omega_e$. In (a) and (c): CP=coupled pseudostate approximation; solid curve B1=exact first Born cross section; dashed curve=IPMB1. In (b): solid surface=CP; wire surface=exact first Born. Except for the exact first Born numbers, all calculations are in the 165 state approximation.

For He we do not have a nice exact analytic expression as in Eq. (77), but we can calculate the wave version of the first Born amplitude in the frozen-core approximation by using Eqs. (59) and (60). This has to be done numerically, breaking Eq. (60) down into partial waves. However, we are able to use as many partial waves as we deem necessary and make the numerical treatment as accurate as possible so that, in effect, we have an exact first Born TDCS within the frozen-core approximation (again we shall call this EXB1). So, once more we are able to make comparison with the first Born treatment in the impact-parameter method (IPMB1) and assess the suitability of the pseudostate basis and the impact-parameter method at this level.

In showing our differential results we have adopted the following conventions. We take the Z direction to be the direction of the incident antiproton. The incident and scattered antiprotons define the X-Z plane with the scattered antiproton coming out on the negative X side. The Cartesian coordinate system is completed with a Y axis to form a right-handed set. In describing the DDCS $d^2\sigma/dEd\Omega_e$ we measure the angle of ejection ($0°-180°$) from the incident antiproton direction.

Finally, all of our differential cross sections are as observed in the laboratory frame of reference.

IV. RESULTS

A. Atomic hydrogen target

In Fig. 2 we show our results for the total ionization cross section in atomic hydrogen. While we have chosen to exhibit the energy range 0.1–500 keV, we would not consider the IPM numbers to be reliable below 1 keV where the approximations inherent in the method become dubious and where trajectory curvature effects appear to be important [27,29].

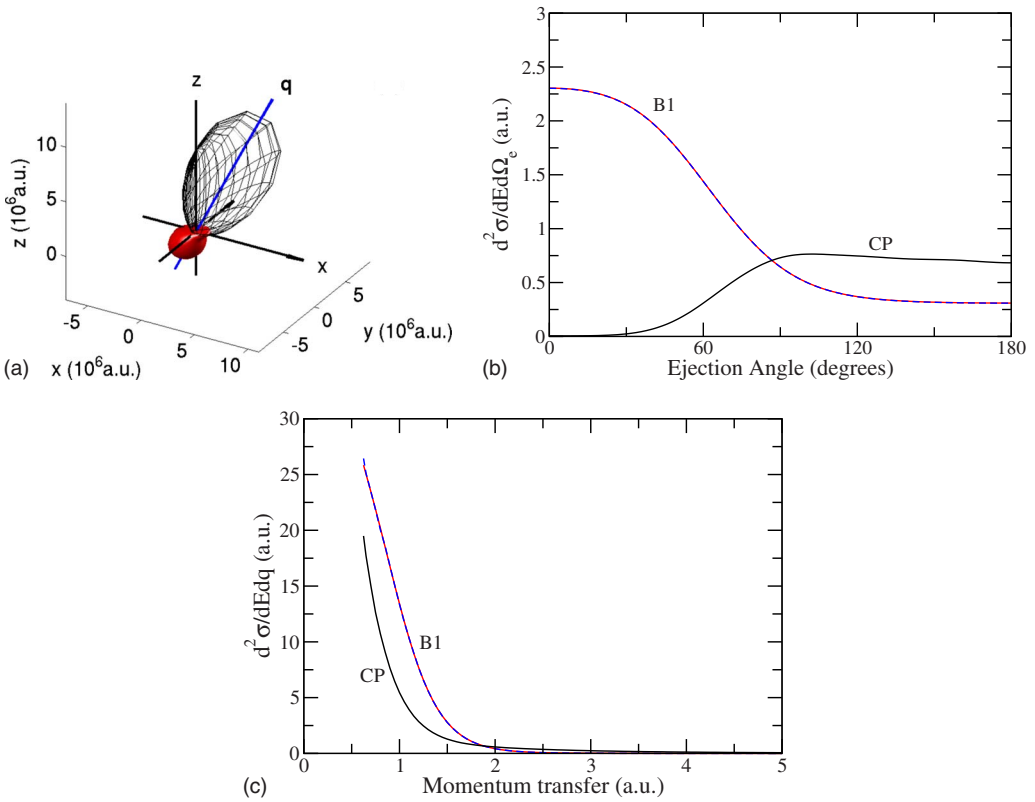

FIG. 4. (Color online) Same as Fig. 3 but for an impact energy of 30 keV: (a) TDCS (q=0.7 a.u.); (b) $d^2\sigma/dEd\Omega_e$; (c) $d^2\sigma/dEdq$. In (b) and (c) the dashed IPMB1 curve is almost indistinguishable from the solid B1 curve representing the exact first Born result.

Rather our purpose is to see what happens in the IPM coupled pseudostate (CP) approximation in the low-energy limit irrespective of its validity there.

We note the following points from Fig. 2: (i) the good agreement between the IPMB1 and EXB1 results, justifying the IPM pseudostate approach at least at the first Born level; (ii) the rapid decline in the first Born cross section at low energies, similar to that seen for CDW-EIS; (iii) the contrasting much larger CP cross section in the low-energy region; (iv) the increasing difference between the 165 and 75 state CP approximations with reducing energy, reflecting upon convergence with respect to the number of pseudostates; (v) the convergence of the theories and the experiment to the first Born limit with increasing energy, adding confidence to all of the results in the high-energy region; (vi) the equally good agreement of the CP and CDW-EIS approximations with experiment within the quoted error bars, showing the need for measurements at lower energies (below about 10 keV) where there are substantial differences between CP and CDW-EIS. Let us look at some of these points in more detail.

To understand the sharp decline in the first Born cross section with reducing energy we must examine its physical content. Because of the orthogonality of the initial and final states, ψ_0 and ψ_f, for ionization, the interaction of the antiproton with the atomic nucleus, $Z_P Z_T/R$ of Eq. (2), does not contribute to the first Born amplitude [Eq. (22)]. Consequently, in this approximation the antiproton can only be scattered by the atomic electron. In Fig. 2 we show the minimum momentum transfer ($q_{\min}$) that is required for ionization at each impact energy. We observe that in the low-energy region, where the first Born cross section is small, $q_{\min}$ becomes large (greater than about 1.5 a.u., say). Clearly, it is the inability of the light target electron to provide sufficiently large momentum transfer to the much heavier antiproton that causes the rapid reduction in the first Born cross section. By contrast, the CP approximation retains the antiproton-nucleus interaction and so is able to sustain a substantial low-energy cross section. This explanation is further supported by the $d^2\sigma/dEdq$ cross sections shown in Figs. 5(b) and 10(b). It is likely, but not absolutely clear, that the same criticism applies to the CDW-EIS approximation. We note that this approximation reduces to a product of factors multiplying the first Born term $|^{B1}R(\eta)|^2$ in formulas (41) and (50) of [65]. Further analysis is needed.

Let us now look at convergence of the CP approximation. Above 10 keV there is very good agreement between the 165 and 75 state approximations, better than 3%. By 1 keV the difference is 12% and by 0.1 keV it is a factor of 2 (see Fig. 2). With allowance for different weighting schemes, to be discussed below, the 165 state approximation is in good agreement with the single center B spline calculations of Azuma *et al.* [31] and Sahoo *et al.* [38] and with the two-center pseudostate calculations of Toshima [30] at 1 keV and above. We therefore have considerable confidence in the convergence of the 165 state approximation for the total ionization cross section at energies above 1 keV. However, as Toshima [30] has shown, there is a rapid deterioration in the rate of convergence of single-center pseudostate expansions, similar to that used here, at energies below 1 keV. At 0.1 keV Azuma *et al.* [31], Sahoo *et al.* [38], and Toshima [30] get

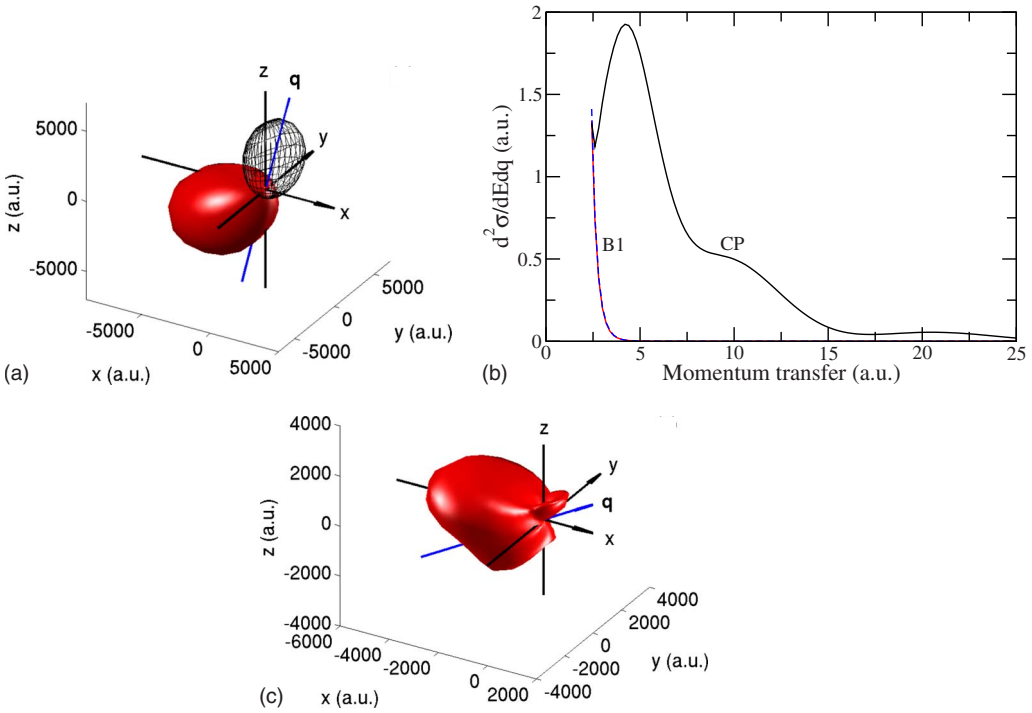

FIG. 5. (Color online) Same as Fig. 3 but for an impact energy of 2 keV: (a) TDCS for $q=2.5$ a.u.; (b) $d^2\sigma/dEdq$; (c) TDCS for $q=5.0$ a.u.. In (c) the first Born cross section is negligible.

cross sections almost twice as large as the 165 state CP approximation shown in Fig. 2.

Different from other coupled state calculations which evaluate the ionization cross section by giving unit weight to each pseudostate with energy above the ionization threshold and zero weight to those below (see, for example, [4,6,31,38]), we use the prescription (73) which weights according to the fraction of the pseudostate lying in the continuum. For the 165 state CP approximation Eq. (73) always gives a lower cross section than the unit weighting, by about 5% at impact energies above 2 keV but increasing to 18% at 0.1 keV. Unfortunately, the first Born approximation, for which we have exact numbers, does not give unambiguous guidance as to which is the better choice. If anything, it suggests that an average of the two options might be best at energies of 10 keV and above.

Let us now look at differential cross sections. Figure 3 shows results at the high impact energy of 500 keV and for an ejected electron energy of 5 eV. Figure 3(a) illustrates the TDCS in the scattering plane for a momentum transfer $q=0.25$ a.u. which is close to the minimum momentum transfer of $q_{\min}=0.15$ a.u.. Here we see almost perfect agreement between EXB1 and the 165 state IPMB1. Similar agreement is also seen in Figs. 3(c), 4(b), and 4(c) where the two results are essentially indistinguishable. Indeed, we get the same almost perfect accord with the 75 state approximation in these cases. One small exception is the $d^2\sigma/dEdq$ cross section of Fig. 5(b) where the 165 state IPMB1 cross section is a little bit larger than EXB1 at the minimum momentum transfer $q_{\min}=2.43$ a.u. but otherwise indistinguishable. Where the distinction between EXB1 and IPMB1 is small, we shall refer to them generically simply as B1. This excellent agreement between EXB1 and IPMB1 considerably strengthens our confidence in the impact-parameter pseudostate approach.

Comparing the B1 results of Fig. 3(a) with CP, we see a pattern that is familiar from $(e,2e)$ [66,67]. Compared with B1, the binary peak of CP is reduced and the recoil peak is enhanced and both are rotated away from the outgoing projectile. This pattern is also seen in the CDW-EIS calculations of Voitkiv and Ullrich [7]. In $(e,2e)$ this behavior is understood as postcollisional interaction (PCI) between the fast outgoing scattered electron and the slow ejected target electron [67]. The only difference in the present case is that the projectile is much heavier but the PCI with the target electron is the same. Figure 3(b) shows the TDCS of Fig. 3(a) in full three dimensions. Note that the B1 TDCS is rotationally symmetric about the direction of momentum transfer $\mathbf{q}$.

Figure 3(c) shows the DDCS $d^2\sigma/dEd\Omega_e$. This cross section samples the TDCS over all angles (equivalently, allowed momentum transfers) of the scattered antiproton. In the figure we see one main peak which in the CP approximation is smaller than B1 and displaced to larger angles. This peak is the "average" of the binary peak seen in Figs. 3(a) and 3(b). Beyond 85° the CP approximation gives a larger cross section than B1, reflecting the enhanced recoil ejection seen in Figs. 3(a) and 3(c). The pattern of Fig. 3(c) bears a resemblance to the single differential cross section $d\sigma/d\Omega_e$ (which is an average of $d^2\sigma/dEd\Omega_e$ over all ejected electron energies) calculated by Igarashi *et al.* [6] for H and Barna *et al.* [8] for He, as one might expect.

Figure 4 shows differential cross sections at 30 keV. This is close to where the B1 and CP total ionization cross sections have their maxima but are significantly different in size, see Fig. 2. Figure 4(a) illustrates the TDCS in three dimensions for $q=0.7$ a.u. ($q_{\min}=0.62$ a.u.). The CP cross section

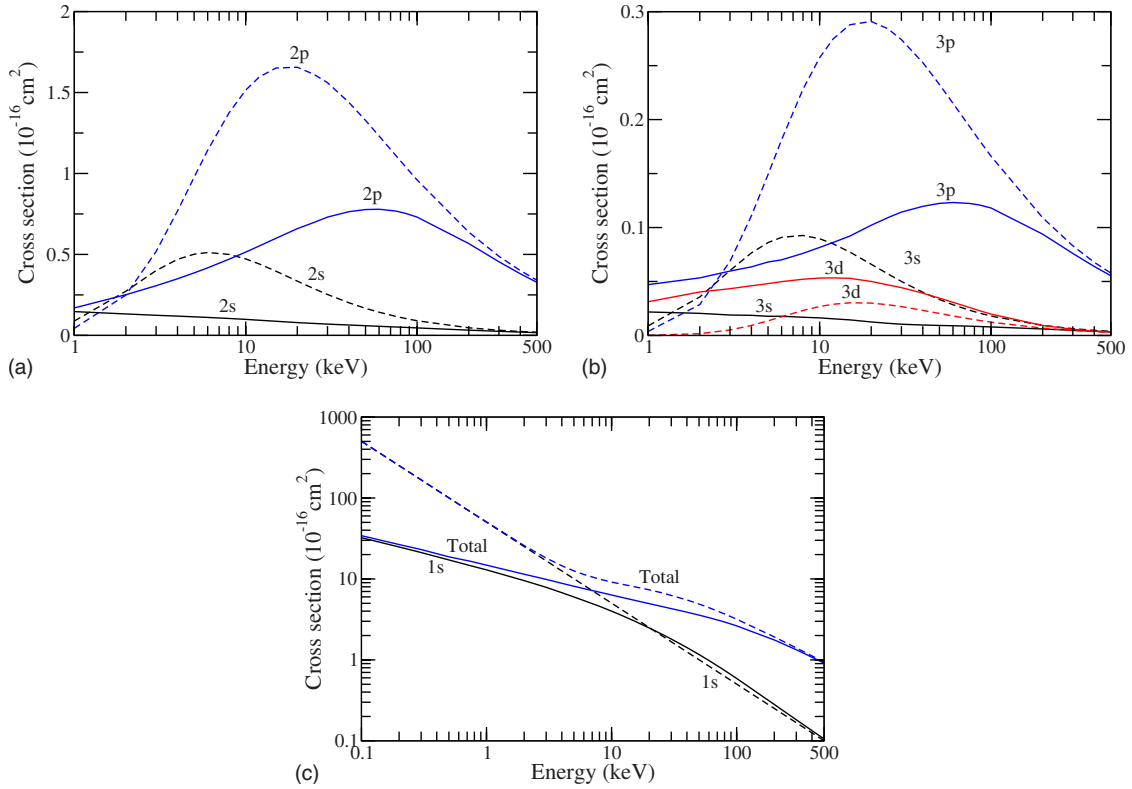

FIG. 6. (Color online) Elastic, excitation and total cross sections: solid curves, 165 state CP approximation; dashed curves, 165 state IPMB1 approximation.

shows the 5 eV ejected electron being strongly repelled by the outgoing antiproton. By contrast, the B1 cross section, which does not contain PCI, points in the opposite direction. The same is seen in Fig. 4(b) for $d^2\sigma/dEd\Omega_e$ where the B1 cross section peaks at the forward direction, while the CP cross section maximizes at backward angles. Figure 4(c) illustrates $d^2\sigma/dEdq$. Here we see a rapid decrease in cross section with increasing q. This pattern of behavior is identified with the high-energy regime. The rapid change in cross section is a warning to experimentalists.

We next pick the impact energy of 2 keV where Fig. 2 shows the B1 cross section to be almost negligible but the CP cross section to be still close to its maximum value. The differential results at this energy are shown in Fig. 5. Figure 5(a) shows the TDCS at $q=2.5$ a.u. ($q_{\min}=2.43$ a.u.). Here the B1 cross section is smaller than CP but still of comparable size. However, its orientation is completely different from CP which, following Fig. 4(a), continues to show strong repulsion of the ejected electron away from the outgoing antiproton. Figure 5(b) shows the DDCS $d^2\sigma/dEdq$. For the CP cross section the picture here is entirely different from the high-energy regime illustrated in Fig. 4(c). While the B1 cross section continues to fall rapidly with increasing q, the CP cross section exhibits a much more sustained variation with q. Initially, like B1, it begins to fall rapidly from $q=q_{\min}$ but then quickly reaches a minimum at $q=2.6$ a.u. It then starts to rise toward a maximum at $q=4.3$ a.u., being there larger even than its value at $q_{\min}$. Even at $q=25.0$ a.u. the CP cross section continues to be nonnegligible. The sustained CP cross section with increasing q reinforces our earlier statement concerning the importance of the projectile-nucleus interaction. Figure 5(c) shows the CP TDCS at $q=5.0$ a.u., i.e., near the maximum in Fig. 5(b). Again we see the effect of Coulomb repulsion on the ejected electron although a larger fraction of the ejected electrons have a component of motion in the incident direction than at $q=2.5$ a.u. We note also the more structured nature of the CP TDCS as compared with Fig. 5(a) and the protrusion in the binary direction.

As remarked elsewhere [56], a great virtue of a coupled pseudostate approach is that it gives a complete picture of all the main processes. In Figs. 6(a) and 6(b) we show the $n=2$ and $n=3$ excitation cross sections that come out of our 165 state CP calculations. Except for some small deviations there is a very good measure of agreement with earlier calculations [6,17,19,24,28]. The agreement with the corresponding 75 state numbers is also impressive, within 1.5% for the $n=2$ excitations above 0.5 keV, within 5% (13%) with the $n=3$ excitations above 10 keV (1 keV). As judged from the first Born approximation, part of the reason (about 3%) for the poorer agreement for the $n=3$ excitations is the more approximate nature of the $n=3$ "eigenstates." Also shown in Figs. 6(a) and 6(b) is the first Born approximation (165 state IPMB1). Here we see substantial differences with the CP calculations but convergence with increasing impact energy. Figure 6(c) shows the 165 state CP elastic cross section and total cross section [Eq. (74)]. In the energy range up to 20 keV elastic scattering greatly outweighs other scatterings. By 500 keV ionization and $2p$ excitation are the dominant contributions to the total cross section and are of com-

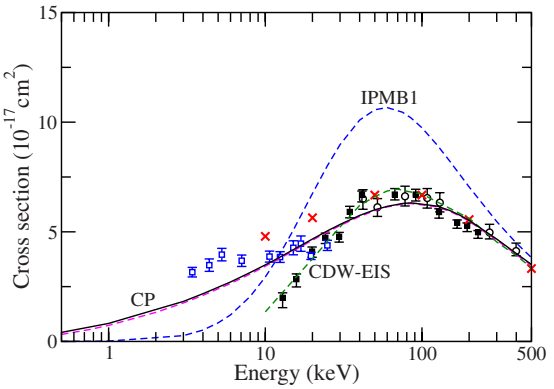

FIG. 7. (Color online) Total ionization cross section for antiproton impact on He: solid (dashed) CP curve, coupled pseudostate IPM calculation with 165 (75) states; IPMB1, first Born cross section in the impact-parameter treatment using the 165 state set; CDW-EIS, continuum distorted wave eikonal initial-state approximation from [10]; crosses, calculations of Igarashi *et al.* [26]; open (solid) circles, experimental data from [46] ([47]); open squares, new experimental data from [45] in the energy range 3–25 keV.

parable size. The CP elastic and total cross sections in the 165 and 75 state approximations are in very good agreement.

B. Helium target

Of the two targets He is experimentally much more feasible. It is therefore important to have results for this case in the literature. They are shown in Figs. 7–11.

Figure 7 shows the total ionization cross section. Here we compare our 165 state CP cross section with the previous CDW-EIS calculation of [10] and with the available experimental data [45–47]. The CDW-EIS cross section follows the older experimental data [46,47] to perfection, in particular it supports the rapid turndown in the measurements at low energies. Very recently, however, new measurements have appeared in the energy range 3.42–24.9 keV [45]. These measurements merge with the older data at the upper end of their energy range but predict a much larger cross section at lower energies, qualitatively in agreement with CP. Quantitatively, the CP cross section agrees with the new measurements between 10 and 17 keV but not at the two highest points and is in equally good agreement as CDW-EIS with the older data above 30 keV. Also shown in Fig. 7 is the IPMB1 approximation. The relative behavior between CP and IPMB1 is similar to that seen in Fig. 2 for H and, again, demonstrates the importance of the projectile-target nucleus interaction in sustaining the ionization cross section at low energies [see also Fig. 10(b)].

Our 75 state CP results are also shown in Fig. 7. They are in very good agreement with the 165 state calculations above 6 keV, being within 2.5%, but deteriorate to 4, 12, and 28% at 3, 1, and 0.5 keV, respectively. With allowance for different pseudostate weightings (see below) there is good agreement between the 165 state cross sections and similar calculations (at 10 keV and above) of Igarashi *et al.* [26] where, as here, one electron is frozen into the $He^+(1s)$ orbital. We therefore feel that, within the context of the frozen $He^+(1s)$

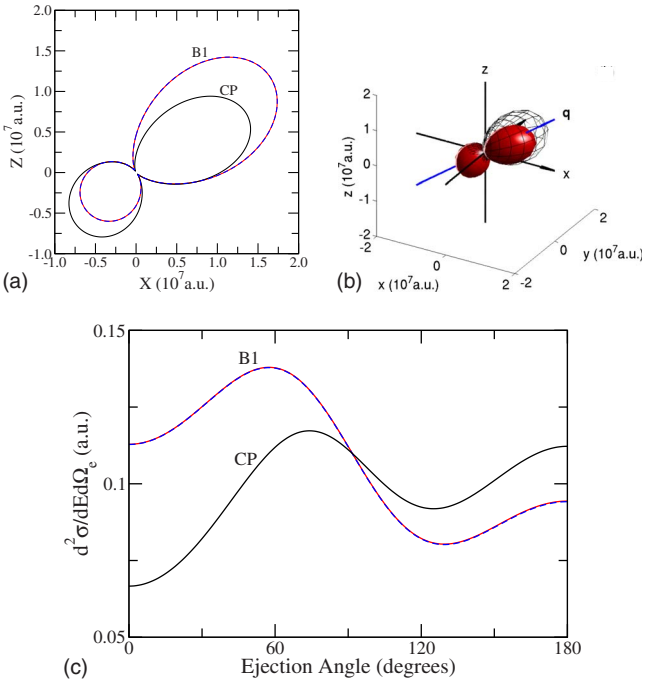

FIG. 8. (Color online) Laboratory frame cross sections (in a.u.) for antiproton ionization of He at 500 keV and for an ejected electron energy of 5 eV: (a) polar plot of TDCS in scattering plane (q=0.40 a.u.); (b) 3D plot of TDCS (q=0.40 a.u.); (c) $d^2\sigma/dEd\Omega_e$. In (a) and (c): CP=coupled pseudostate approximation; solid curve B1=exact first Born cross section in the frozen-core approximation (EXB1); dashed curve=IPMB1. In (b): solid surface=CP; wire surface=exact first Born EXB1. With the exception of the ionized state in EXB1 [see Eq. (60)], all calculations are in the 165 state approximation. In EXB1 the He ground-state wave function and energy of the 165 state approximation have been used.

model, our 165 state calculations of the total ionization cross section are well converged, at the very least in the energy range from 3 keV upwards. Instead of employing Eq. (73), using a weighting of unity for pseudostates with energies above −2.0 a.u., and zero for those below, raises our CP ionization cross section by about 3% above 12 keV and by 5, 8, and 11% at 3, 1, and 0.5 keV, respectively. This is insufficient to explain the differences with the most recent experimental data [45] shown in Fig. 7. Igarashi *et al.* [26] also made calculations with states which include the n=2 and n=3 He^+ orbitals. Compared with the frozen $He^+(1s)$ results, their ionization cross section at 10 keV is raised by about 30%, reducing to 20% and 7% at 20 and 50 keV, respectively, and being negligibly different at still higher energies. These cross sections are shown in Fig. 7. At 50 keV and below these cross sections are in good agreement with the very recent calculations of Foster *et al.* [44] who solved the time-dependent Schrödinger equation on a grid treating both electrons equally. The results of Igarashi *et al.* [26] and Foster *et al.* [44] imply that the frozen $He^+(1s)$ model, as used here, is not so reliable below about 50 keV. However, as we see from Fig. 7, the cross sections of Igarashi *et al.* [26] (and so also Foster *et al.* [44]) are in even worse agreement with the new experimental data of [45] than our present CP results. It is not clear whether it is experiment or theory which is at fault.

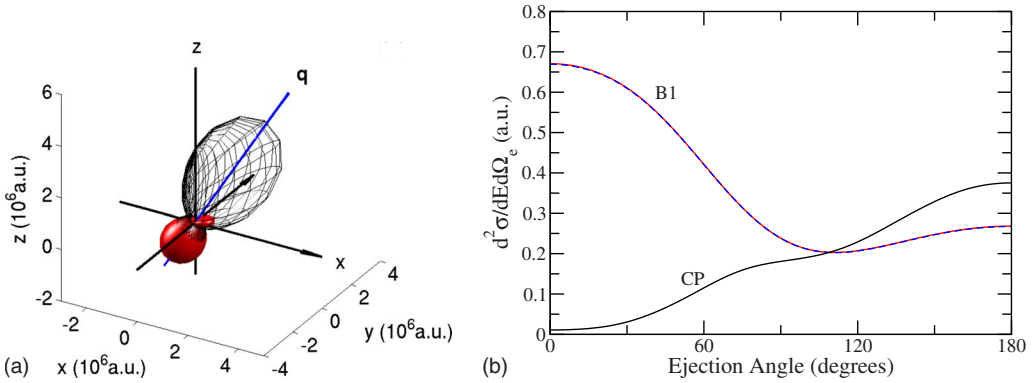

FIG. 9. (Color online) Same as Fig. 8 but for an impact energy of 60 keV: (a) TDCS (q=0.80 a.u.); (b) $d^2\sigma/dEd\Omega_e$. In (b) the dashed IPMB1 curve is almost indistinguishable from the solid B1 curve representing the exact first Born result.

In Figs. 8–10 we show a selection of differential cross sections in the 165 state approximation for He. Following Figs. 3–5 for H, we have chosen a high energy (500 keV, Fig. 8), an energy near the maximum in the CP total ionization cross section (60 keV, Fig. 9), and a low energy where the first Born approximation to the total ionization cross section is negligible (3 keV, Fig. 10). Although our frozen $He^+(1s)$ approximation is not valid at 3 keV, see remarks above, we think it worthwhile to see what happens in this model, if only to compare against H. From Figs. 8–10 we see the same pattern of behavior as for H but with some differences in detail. Following the case of H, we note the sustained CP cross section $d^2\sigma/dEdq$ at 3 keV [Fig. 10(b)], showing, once more, the importance of large momentum-transfer scattering at low energies, and the excellent agreement of the exact first Born approximation EXB1 with the corresponding impact-parameter results IPMB1 (and also with the 75 state IPMB1, not shown) at 500 and 60 keV.

Finally, for completeness, we show in Fig. 11 the 165 state cross sections, CP and IPMB1, for elastic scattering and for the discrete excitations $2^1S, 2^1P, 3^1S, 3^1P, 3^1D$, as well as the total cross section Eq. (74). Our results are in good agreement with the earlier work of Igarashi *et al.* [26] in the frozen-core approximation. With the exception of the n=3 excitations, there is also excellent agreement with the 75 state approximation. For the n=3 transitions there can be differences between the 75 and 165 state calculations of up to 4% at energies above 10 keV, with larger excursions up to 20% at energies down to 1 keV. Igarashi *et al.* [26] have shown to what extent the discrete excitation cross sections can be affected by the frozen-core assumption, for the P and D transitions generally not that much, for the S transitions more substantially.

V. CONCLUSIONS

In this paper we have developed a method for extracting fully differential cross sections for ionization from an impact-parameter treatment of the collision. The approach uses pseudostates to represent the ionized continuum. We have employed the first Born approximation in the wave form as a check on the method and found excellent agreement at the first Born level. However, the first Born approximation cannot tell us the whole story; it provides a necessary but not sufficient test. The method is, of course, not restricted to antiprotons and may be used with other projectiles, e.g., C^{6+}, Au^{24+}, and Au^{53+}, for which we hope to announce results soon. An important aspect of the method is that it automatically includes the interaction between the projectile and the target nucleus in a natural way and without further approximation. We have seen the importance of this interaction in the low-energy antiproton ionization [Figs. 5(b) and 10(b)]. This feature of the method is relevant to ongoing questions concerning the importance of projectile-nucleus scattering in differential ionization studies [68]. The present

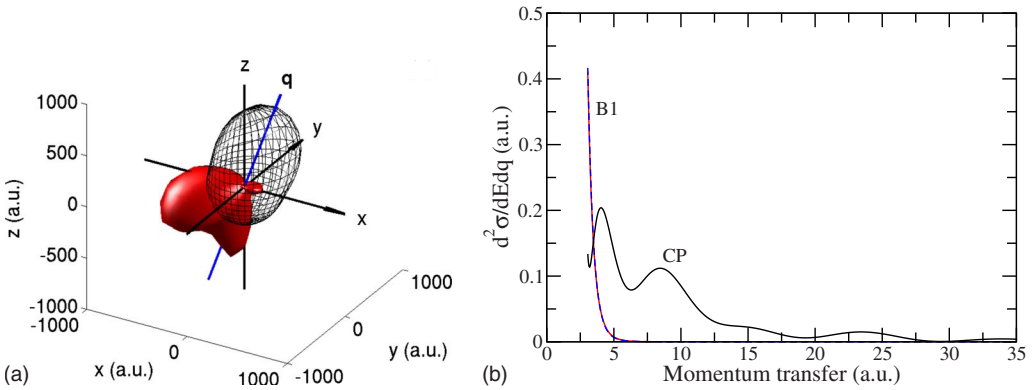

FIG. 10. (Color online) Same as Fig. 8 but for an impact energy of 3 keV: (a) TDCS (q=3.25 a.u.); (b) $d^2\sigma/dEdq$.

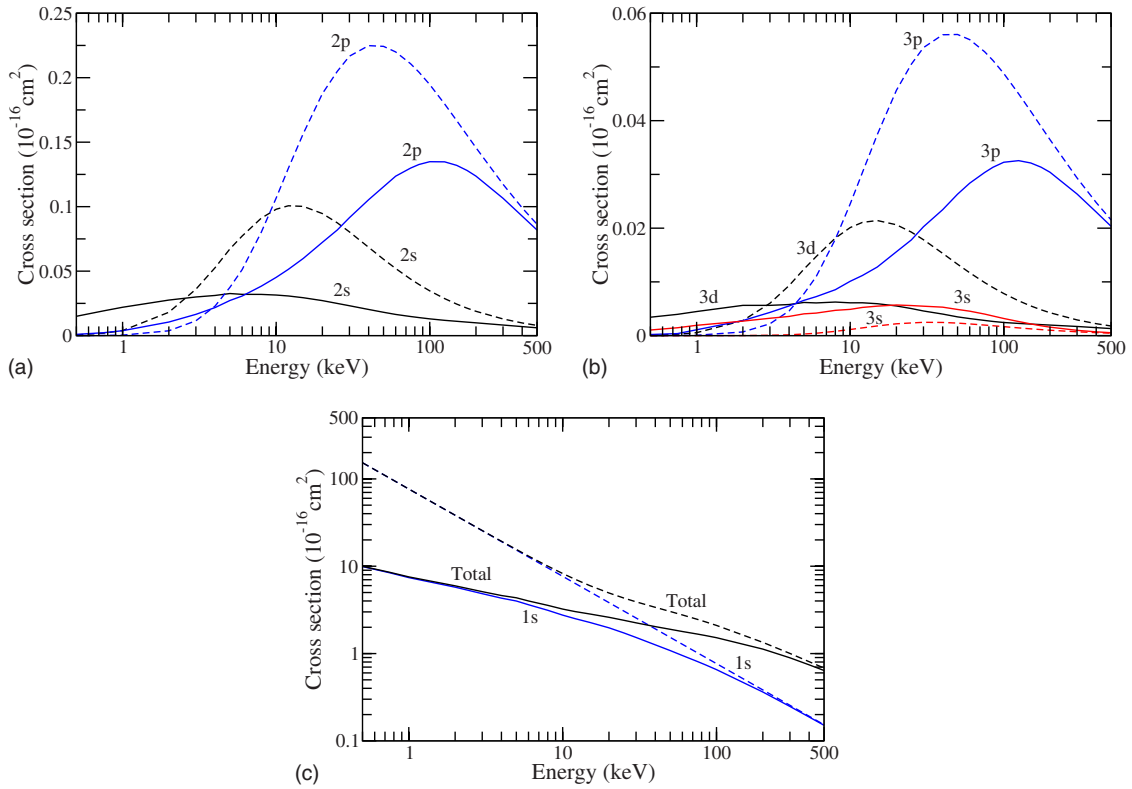

FIG. 11. (Color online) Elastic, excitation and total cross sections: solid curves, 165 state CP approximation; dashed curves, 165 state IPMB1 approximation.

approach should be able to answer these questions in a convincing way.

As a by-product of the differential calculations we have also evaluated the total cross sections for ionization and some important discrete excitations. As remarked elsewhere [56], this is a strength of the pseudostate approach, namely, that it is able to give a complete and internally consistent picture of all the main processes. Until very recently, the experimental data for total single ionization of He [46,47] gave a much smaller cross section at the lower energies than was predicted by the more sophisticated theories [41] but, paradoxically, were in almost perfect agreement with a simpler CDW-EIS approximation. The present work supports the earlier sophisticated theories and suggests that, like the first Born approximation, the CDW-EIS results are too low because they fail to take adequate account of the interaction of the projectile with the atomic nucleus. The most recent experimental data on He [45] give a larger cross section at low energies than the older measurements but still fail to provide convincing agreement with the available theories. It is unclear as to what extent it is theory and/or experiment that is at fault.

The experimental and theoretical situations for ionization at the higher energies appear to be essentially satisfactory for both H and He. This energy range therefore provides a good test bed for new experimental developments, e.g., differential measurements. However the really interesting region lies at lower energies, below 30 keV. Here total ionization measurements for H would be particularly welcome, see Fig. 2, but what would be really enlightening, in this energy region, would be differential measurements on H and/or He. These, we believe, would probe some very interesting mechanisms involving the relative interplay of the interactions between the antiproton, ionized electron, and nucleus as the impact energy is changed.

ACKNOWLEDGMENTS

One of us (M.McG.) acknowledges support from the European Social Fund . D.A. and J.R.M. acknowledge financial support from the Brazilian agencies CNPq, Capes, and Fapemig. We are also indebted to H. Knudsen *et al.* [45] for sending us tabulated values of their measurements.

[1] R. E. Olson and T. J. Gay, Phys. Rev. Lett. **61**, 302 (1988).
[2] E. Y. Sidky and C. D. Lin, J. Phys. B **31**, 2949 (1998).
[3] Kh. Khayyat, T. Weber, R. Dörner, M. Achler, V. Mergel, L. Spielberger, O. Jagutzki, U. Meyer, J. Ullrich, R. Moshammer, W. Schmitt, H. Knudsen, U. Mikkelsen, R. Aggerholm, E. Uggerhoej, S. P. Moeller, V. D. Rodríguez, S. F. C. O'Rourke, R. E. Olsen, P. D. Fainstein, J. H. McGuire, and H. Schmidt-Böcking, J. Phys. B **32**, L73 (1999).
[4] B. Pons, Phys. Rev. Lett. **84**, 4569 (2000).
[5] B. Pons, Phys. Rev. A **63**, 012704 (2000).
[6] A. Igarashi, S. Nakazaki, and A. Ohsaki, Phys. Rev. A **61**, 062712 (2000).
[7] A. B. Voitkiv and J. Ullrich, Phys. Rev. A **67**, 062703 (2003).
[8] I. F. Barna, K. Tőkési, L. Gulyas, and J. Burgdörfer, Radiat. Phys. Chem. **76**, 495 (2007).
[9] M. H. Martir, A. L. Ford, J. F. Reading, and R. L. Becker, J. Phys. B **15**, 1729 (1982).
[10] P. D. Fainstein, V. H. Ponce, and R. D. Rivarola, Phys. Rev. A **36**, 3639 (1987).
[11] D. R. Schultz, Phys. Rev. A **40**, 2330 (1989).
[12] G. Schiwietz, Phys. Rev. A **42**, 296 (1990).
[13] M. Kimura, I. Shimamura, and M. Inokuti, Phys. Rev. A **49**, R4281 (1994).
[14] G. Schiwietz, U. Wille, R. Díez Muiño, P. D. Fainstein, and P. L. Grande, J. Phys. B **29**, 307 (1996).
[15] D. R. Schultz, P. S. Krstić, C. O. Reinhold, and J. C. Wells, Phys. Rev. Lett. **76**, 2882 (1996).
[16] P. S. Krstić, D. R. Schultz, and R. K. Janev, J. Phys. B **29**, 1941 (1996).
[17] J. C. Wells, D. R. Schultz, P. Gavras, and M. S. Pindzola, Phys. Rev. A **54**, 593 (1996).
[18] L. A. Wehrman, A. L. Ford, and J. F. Reading, J. Phys. B **29**, 5831 (1996).
[19] K. A. Hall, J. F. Reading, and A. L. Ford, J. Phys. B **29**, 6123 (1996).
[20] T. Das and F. B. Malik, J. Phys. B **30**, 1223 (1997).
[21] J. F. Reading, T. Bronk, A. L. Ford, L. A. Wehrman, and K. A. Hall, J. Phys. B **30**, L189 (1997).
[22] G. Bent, P. S. Kristić, and D. R. Schultz, J. Chem. Phys. **108**, 1459 (1998).
[23] T. Bronk, J. F. Reading, and A. L. Ford, J. Phys. B **31**, 2477 (1998).
[24] T. Kirchner, H. J. Lűdde, O. J. Kroneisen, and R. M. Dreizler, Nucl. Instrum. Methods Phys. Res. B **154**, 46 (1999).
[25] T. G. Lee, H. C. Tseng, and C. D. Lin, Phys. Rev. A **61**, 062713 (2000).
[26] A. Igarashi, A. Ohsaki, and S. Nakazaki, Phys. Rev. A **62**, 052722 (2000).
[27] K. Sakimoto, J. Phys. B **33**, 3149 (2000).
[28] K. Sakimoto, J. Phys. B **33**, 5165 (2000).
[29] X.-M. Tong, T. Watanabe, D. Kato, and S. Ohtani, Phys. Rev. A **64**, 022711 (2001).
[30] N. Toshima, Phys. Rev. A **64**, 024701 (2001).
[31] J. Azuma, N. Toshima, K. Hino, and A. Igarashi, Phys. Rev. A **64**, 062704 (2001).
[32] X.-M. Tong, T. Watanabe, D. Kato, and S. Ohtani, Phys. Rev. A **66**, 032708 (2002).
[33] X.-M. Tong, T. Watanabe, D. Kato, and S. Ohtani, Phys. Rev. A **66**, 032709 (2002).
[34] T. Kirchner, M. Horbatsch, E. Wagner, and H. J. Lüdde, J. Phys. B **35**, 925 (2002).
[35] D. R. Schultz and P. S. Krstić, Phys. Rev. A **67**, 022712 (2003).
[36] I. F. Barna, N. Grün, and W. Scheid, Eur. Phys. J. D **25**, 239 (2003).
[37] M. Keim, A. Achenbach, H. J. Lüdde, and T. Kirchner, Phys. Rev. A **67**, 062711 (2003).
[38] S. Sahoo, S. C. Mukherjee, and H. R. J. Walters, J. Phys. B **37**, 3227 (2004).
[39] A. Igarashi, S. Nakazaki, and A. Ohsaki, Nucl. Instrum. Methods Phys. Res. B **214**, 135 (2004).
[40] T. Morishita, T. Sasajima, S. Watanabe, and M. Matsuzawa, Nucl. Instrum. Methods Phys. Res. B **214**, 144 (2004).
[41] S. Sahoo, S. C. Mukherjee, and H. R. J. Walters, Nucl. Instrum. Methods Phys. Res. B **233**, 318 (2005).
[42] S. Yu. Ovchinnikov and J. H. Macek, Phys. Rev. A **71**, 052717 (2005).
[43] G. Lapicki, Nucl. Instrum. Methods Phys. Res. B **241**, 34 (2005).
[44] M. Foster, J. Colgan, and M. S. Pindzola, Phys. Rev. Lett. **100**, 033201 (2008).
[45] H. Knudsen, H.-P. E. Kristiansen, H. D. Thomsen, U. I. Uggerhøj, T. Ichioka, S. P. Møller, C. A. Hunniford, R. W. McCullough, M. Charlton, N. Kuroda, Y. Nagata, H. A. Torii, Y. Yamazaki, H. Imao, H. H. Andersen, and K. Tökesi, Phys. Rev. Lett. **101**, 043201 (2008).
[46] L. H. Andersen, P. Hvelplund, H. Knudsen, S. P. Møller, J. O. P. Pedersen, S. Tang-Petersen, E. Uggerhøj, K. Elsener, and E. Morenzoni, Phys. Rev. A **41**, 6536 (1990).
[47] P. Hvelplund, H. Knudsen, U. Mikkelsen, E. Morenzoni, S. P. Møller, E. Uggerhøj, and T. Worm, J. Phys. B **27**, 925 (1994).
[48] M. E. Rose, *Elementary Theory of Angular Momentum* (Wiley, New York, 1957).
[49] Under the circumstances envisaged here, where the directions of $\mathbf{k}_0$ and $\mathbf{k}_f$ differ only by milliradians and where we shall neglect terms of order $\frac{1}{\mu}$, it matters not whether we take the z direction along $\mathbf{k}_0+\mathbf{k}_f$ or $\mathbf{k}_0$ or $\mathbf{k}_f$. The more "symmetrical" choice $\mathbf{k}_0+\mathbf{k}_f$ makes the argument more "elegant."
[50] I. S. Gradshteyn and I. M. Ryzhik, *Table of Integrals, Series, and Products*, 7th ed. (Academic, New York, 2007).
[51] R. H. G. Reid, A. E. Kingston, and M. J. Jameson, J. Phys. B **10**, 55 (1977).
[52] H. R. J. Walters, J. Phys. B **21**, 1277 (1988).
[53] We do not need the i label here.
[54] Our angular momentum conventions are those of Rose [48]. The asterisk denotes complex conjugate.
[55] This is not to imply that the ψ_{nlm} are bound eigenstates. They are a mixture of eigenstates and pseudostates.
[56] H. R. J. Walters, J. E. Blackwood, and M. T. McAlinden, in *New Directions in Antimatter Chemistry and Physics*, edited by C. M. Surko and F. A. Gianturco (Kluwer, Dordrecht, 2001), p. 173.
[57] W. C. Fon, K. A. Berrington, P. G. Burke, and A. E. Kingston, J. Phys. B **14**, 1041 (1981).
[58] For ionization, $(\varepsilon_f-\varepsilon_0)=\frac{\kappa^2}{2}+I$, where I is the ionization potential, and $k_f^2=k_0^2-\mu(\kappa^2+2I)$.
[59] I. Bray and A. T. Stelbovics, Phys. Rev. A **46**, 6995 (1992).
[60] While for differential ejection studies it is necessary to fix λ_l so that the pseudostates of a particular n manifold have the ejected energy, other aspects of the calculations, such as total

cross sections, are insensitive to the precise values of λ_l as along as enough basis functions are used.
[61] For the Higher values of l the electron moves well beyond the He^+ core and so λ_l tends to the values for H.
[62] G. W. F. Drake and W. C. Martin, Can. J. Phys. **76**, 679 (1998).
[63] J. P. Coleman, in *Case Studies in Atomic Collision Physics I*, edited by E. W. McDaniel and M. R. C. McDowell (North-Holland, Amsterdam, 1969), p. 101.
[64] H. Knudsen, U. Mikkelsen, K. Paludan, K. Kirsebom, S. P. Møller, E. Uggerhøj, J. Slevin, M. Charlton, and E. Morenzoni, Phys. Rev. Lett. **74**, 4627 (1995).
[65] D. S. F. Crothers and J. F. McCann, J. Phys. B **16**, 3229 (1983).
[66] E. P. Curran and H. R. J. Walters, J. Phys. B **20**, 337 (1987).
[67] H. R. J. Walters, X. Zhang, and C. T. Whelan, in *(e, 2e) and Related Processes*, edited by C. T. Whelan, H. R. J. Walters, A. Lahmam-Bennani, and H. Ehrhardt (Kluwer, Dordrecht, 1993), p. 33.
[68] M. Schulz, M. Dürr, B. Najjari, R. Moshammer, and J. Ullrich, Phys. Rev. A **76**, 032712 (2007).